Carbohydrate Polymers 134 (2015) 467–474

Contents lists available at ScienceDirect

Carbohydrate Polymers

journal homepage: www.elsevier.com/locate/carbpol

# High-throughput and high-yield fabrication of uniaxially-aligned chitosan-based nanofibers by centrifugal electrospinning

Ariane E. Erickson[1], Dennis Edmondson[1], Fei-Chien Chang, Dave Wood, Alex Gong, Sheeny Lan Levengood, Miqin Zhang*

*Department of Materials Science and Engineering, University of Washington, Seattle, WA 98195, USA*

ARTICLE INFO

*Article history:*
Received 22 April 2015
Received in revised form 29 July 2015
Accepted 30 July 2015
Available online 1 August 2015

*Keywords:*
Centrifugal electrospinning
High-throughput
Alignment
Nanofibers

ABSTRACT

The inability to produce large quantities of nanofibers has been a primary obstacle in advancement and commercialization of electrospinning technologies, especially when aligned nanofibers are desired. Here, we present a high-throughput centrifugal electrospinning (HTP-CES) system capable of producing a large number of highly-aligned nanofiber samples with high-yield and tunable diameters. The versatility of the design was revealed when bead-less nanofibers were produced from copolymer chitosan/polycaprolactone (C-PCL) solutions despite variations in polymer blend composition or spinneret needle gauge. Compared to conventional electrospinning techniques, fibers spun with the HTP-CES not only exhibited superior alignment, but also better diameter uniformity. Nanofiber alignment was quantified using Fast Fourier Transform (FFT) analysis. In addition, a concave correlation between the needle diameter and resultant fiber diameter was identified. This system can be easily scaled up for industrial production of highly-aligned nanofibers with tunable diameters that can potentially meet the requirements for various engineering and biomedical applications.



## 1. Introduction

Electrospinning is a versatile fabrication technique used to produce fibers with diameters on the order of tens of nanometers to microns while allowing for unprecedented control over diameter, length, alignment, and morphology. This technique has been successfully applied to produce various nanofibrous structures (i.e., beaded, ribbon, core and shell, hollow tube, and porous) using a wide range of polymers and polymeric composites (Ramakrishna et al., 2006). Due to the inexpensive experimental set up and superior versatility in resultant fiber composition, electrospinning remains a dominant area of research over other nanofiber fabrication methods, such as drawing (Suzuki, Hosoi, & Miyagi, 2015), thermally-induced phase separation (Zhang, Liu, Yang, & Zhu, 2015), vapor phase polymerization (D'Arcy et al., 2014), self-assembly (Wan, Yang, Xiong, Raman, & Luo, 2015), and template directed synthesis (Wan et al., 2015). The high surface-to-volume ratio and anisotropy of electrospun nano-scale fibers have proven advantageous in many applications including liquid filtration (Balamurugan, Sundarrajan, & Ramakrishna, 2011), energy storage (Guo et al., 2009; Hiralal et al., 2010), drug delivery (Cui, Zhou, & Chang, 2010; Ignatious, Sun, Lee, & Baldoni, 2010), piezoelectric devices (Chang, Dommer, Chang, & Lin, 2012; Edmondson, Cooper, Jana, Wood, & Zhang, 2012), and biological wound healing (Zahedia, Rezaeiana, Ranaei-Siadatb, Jafaria, & Supapholc, 2012). Two nanofiber properties that are especially important for success in these applications are uniform diameters and high degrees of fiber alignment.

Despite significant progress made in this field in the past decade, challenges remain in the widespread commercialization of electrospinning technologies. The main impediment is the limited throughput of nanofiber production using currently established methods. Thus, there is an urgent need for development of new electrospinning systems suitable for the large-scale production of high-quality nanofibers in a controlled manner. The primary barrier to effective system scale-up is largely due to the complex interplay of the operating parameters such as electric field, electrostatic charging of the polymer, and solvent volatilization, which make it difficult to increase the throughput while maintaining optimized and uniform fiber production (Thoppey, Bochinski, Clarke, & Gorga, 2011). In addition, mass production often results in increased sample loss during the collection process. The product

* Corresponding author at: 302L Roberts Hall, Department of Materials Science and Engineering, University of Washington, Seattle, WA 98195, USA. Fax: +1 206 543 3100.
*E-mail address:* mzhang@u.washington.edu (M. Zhang).
[1] These authors contributed equally to this work.

http://dx.doi.org/10.1016/j.carbpol.2015.07.097
0144-8617/

of high-throughput electrospinning systems is generally a nanofibrous mat collected on a large plate or substrate (Jirsak, Sysel, Sanetrnik, Hruza, & Chaloupek, 2010; Kumar, Wei, Barry, Chen, & Mead, 2010; Lukas, Sarkar, & Pokorny, 2008; Varabhas, Chase, & Reneker, 2008; Varesano, Rombaldoni, Mazzuchetti, Tonina, & Comottob, 2010). Removal of the mat from the substrate without nanofiber loss can present a challenge. Subsequently, handling and cutting the mat into samples of useful size often leads to a compromised nanofiber structure. Overall efficiency of the collection process can be very low due to the number of associated steps.

In conjunction with increased throughput, production of nanofibers with controlled orientation is desirable. For example, aligned nanofibers are particularly useful for tissue engineering applications where they have been shown to improve cell proliferation (Cooper, Jana, Bhattarai, & Zhang, 2010), migration (Ghasemi-Mobarakeh, Prabhakaran, Morshed, Nasr-Esfahani, & Ramakrishna, 2008; Patel et al., 2007), and differentiation (Yin et al., 2010). The most common methods for attaining fiber alignment are exploitation of a rotating drum collector (Matthews, Wnek, Simpson, & Bowlin, 2002; Theron, Zussman, & Yarin, 2001) or a parallel-electrode collector (Baji, Mai, Wong, Abtahi, & Chen, 2010; Li, Wang, & Xia, 2004) where nanofibers selectively align across an insulating gap between two electrodes. Although both of these techniques produce aligned nanofibers, the sample size or fiber length is limited. To overcome both of these limitations, a centrifugal electrospinning (CES) system was introduced to accommodate the need for production of highly aligned fibers over a large area (Edmondson et al., 2012). Using the CES, fibers were deposited across an insulating gap that could be adjusted to obtain fibers up to tens of centimeters in length. Nevertheless, this system was unable to produce a large number of samples of these highly aligned nanofibers. In addition, cutting a large-size nanofiber mat into smaller samples of useful size can be challenging and often leads to compromised nanofiber alignment. Furthermore, only a small portion (~20%) of ejected polymer was deposited between the electrode gaps as aligned nanofibers while the majority was deposited on the large electrode plates as unaligned nanofibers, thus unusable in designated applications, and thereby significantly reducing the nanofiber yield.

While electrospinning has been extensively investigated, a system capable of fabricating a large number of highly-aligned nanofiber samples has not been demonstrated. Here, we present a high-throughput centrifugal-electrospinning (HTP-CES) system that combines the principles of centrifugal spinning and electrospinning using a special configuration of wire electrodes capable of producing highly aligned nanofibers with large sample volume and quantity. Notably, this design allows simultaneous production of aligned nanofibrous mats at 102-collection sites and yet, as a result of the small-wire electrode configuration of the collector, nearly all the ejected polymer was deposited in the electrode gap as collectable, highly-aligned nanofibers, with a production yield of nearly 75%. We electrospun natural/synthetic copolymer blend nanofibers across a range of chitosan and polycaprolactone (C-PCL) polymer blend compositions to illustrate the versatility of the HTP-CES. C-PCL blend nanofibers are highly advantageous for tissue engineering applications due to the favorable combination of the mechanical strength of PCL and the biocompatibility of chitosan (Bhattarai et al., 2009; Sionkowska, 2011). We investigated how parameters such as polymer concentration, centrifugal force, and needle gauge affect the morphology and alignment of resultant C-PCL nanofibers. Furthermore, we investigated if changing the needle gauge size can fine tune fiber diameter in highly-aligned nanofiber samples.

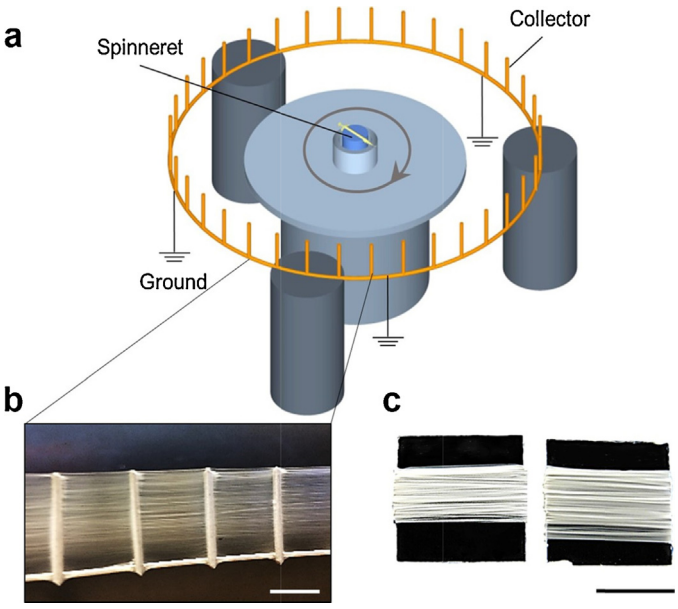


**Fig. 1.** HTP-CES configuration for high-throughput production of highly aligned polymer nanofibers. (a) Schematic representation of the system configuration depicting a rotating, centrifugally-fed spinneret and grounded 102- prong metal wire collector atop three wooden insulating stands. (b) Nanofibers aligned horizontally across four sets of wire electrodes. The scale bar represents 1 cm. (c) C/PCL nanofibers collected onto glass coverslips from the gaps between two wire electrodes on the collector. The scale bar represents 5 mm.

## 2. Materials and methods

### 2.1. System configuration

The primary components of the high-throughput centrifugal-electrospinning (HTP-CES) system include a syringe-needle spinneret driven by a variable speed DC electric motor (Amtek, Monrovia, CA) and a circular 40.5 cm-diameter multiple-pole collector mounted on wooden insulating columns. A 25 kV DC negative high-voltage power supply (HV350REG, Information Unlimited, Amherst, NH) was connected to the spinneret placed at the center of the circular collector (Fig. 1a). The needle tip of the spinneret was 10.7 cm away from the collector and the collector had 102-grounded wire electrodes spaced 1.27 cm apart. Using a high voltage power supply, the solution is charged and fed to the system using the centrifugal force created by the rotation of the spinneret. As the solution is ejected, the jet experiences both axial and tangential stretching as the solvent evaporates and fibers attach to the wire electrode. The rotational movement of the spinneret induces elongation and minimizes the “whipping region” allowing deposition of nanofibers perpendiculuar to the wires, and alignment across the wire gap (Fig. 1b). The nanofibers can be harvested directly from the wire gaps onto glass coverslips (Fig. 1c). This system can also operate in a conventional electrospinning (ES) mode, when the spinneret is held stationary.

### 2.2. Synthesis of C-PCL nanofibers via HTP-CES

Previously optimized polymer stock solutions were utilized to electrospin C-PCL copolymer blend nanofibers with some alterations (Cooper, Bhattarai, & Zhang, 2011). All chemicals were purchased from Sigma Aldrich, St. Louis, MO unless otherwise stated. First, the stock solutions of chitosan and PCL were prepared separately and then mixed to create four C-PCL blend solutions of different ratios of chitosan to PCL. Chitosan (75–85% deacetylated, medium molecular weight (200–800 cP) in 1 wt% acetic acid

at 25 °C) was dissolved in trifluoroacetic acid (TFA) (Fisher, Reagent, ≥97%) to yield a 7 wt% solution that was heated and held at 60 °C for 12 h under constant stirring. A 12 wt% polycaprolactone (PCL) (Average $M_n$ 80,000) solution was prepared by dissolving PCL in 2,2,2-trifluoroethanol (TFE) (ReagentPlus®, ≥99%) overnight under constant stirring at room temperature. The chitosan and PCL stock solutions were combined to form blend solutions that resulted in final nanofiber compositions ranging from 10 wt% chitosan and 90 wt% PCL (10/90C-PCL) to 90 wt% chitosan and 10 wt% PCL (90/10C-PCL). The chitosan and PCL were mixed immediately prior to electrospinning and refreshed every hour to prevent polymer degradation. Consistent environmental conditions were maintained throughout these experiments using a humidifier or dehumidifier to maintain the humidity at 40–50% and the room temperature remained at 20–25 °C.

Four copolymer blend electrospinning solutions (10/90C-PCL, 25/75C-PCL, 75/25C-PCL, and 90/10C-PCL) were utilized to investigate the relationship between copolymer blend composition and nanofiber morphology. Each solution was centrifugally-fed from the spinneret of the HTP-CES using a 24-gauge blunt tip needle. For all solution conditions, a negative DC voltage of 5 kV was applied between the spinneret needle and ground. The spinneret rotational speed was held constant at 108 rpm.

The effect of the centrifugal force on nanofiber morphology and alignment was studied using a 25/75C-PCL solution. Using the HTP-CES modality, where the centrifugal force was applied, the spinneret was rotated at 108 rpm. The spinneret was held stationary for the electrospinning modality (ES) where no centrifugal force was involved. The solution was fed to the system with a voltage of 5 kV and a 24-gauge blunt tip needle for both conditions.

A 25/75C-PCL solution was centrifugally-fed from the spinneret of the HTP-CES, and electrospun using blunt tip needles with five different inner diameters (18, 21, 24, 27, and 30-gauge) to investigate the effect of needle gauge on fiber diameter and alignment. All five conditions were subjected to a voltage of 5 kV and spinneret rotation at 108 rpm.

### 2.3. Characterization of fiber morphology using scanning electron microscopy (SEM)

Using double-sided carbon tape, nanofibers were gathered from the collector onto a pedestal, sputter-coated with Au/Pd for 40 s at 18 mA, and imaged with a FEI Sirion XL30 SEM at an operating voltage of 3 kV.

### 2.4. Chemical characterization using Fourier transform infrared spectroscopy (FTIR)

FTIR spectroscopic analysis of chitosan and PCL as well as polymer blends was performed using a Nicolet 5DXB spectrometer (Thermo Scientific, Boston, MA). A few drops of each solution of chitosan in TFA, PCL in TFE, and C-PCL in TFA/TFE were added to one KBr salt plate with a second plate on top, and analyzed by averaging 64 scans at a resolution of 2 $cm^{-1}$ over a range of 400–4000 $cm^{-1}$.

### 2.5. Determination of solution viscosity

Rheological studies were conducted using a stress-controlled rheometer (MCR 301, Anton Paar, Germany) with a cone and plate configuration of 49.963 mm diameter and 1.008° cone angle. Stock solutions of chitosan-TFA, PCL-TFE, and C-PCL blends (90/10, 75/25, 25/75, and 10/90 chitosan/PCL) were prepared immediately before the measurement. A layer of mineral oil was applied on top of the polymer solution to minimize solution drying. The viscosity was measured as a function of shear rate as shear rate was increased from 10 to 1000 $s^{-1}$ in a dynamic rotatory mode with temperature maintained at 20 °C.

### 2.6. Quantification of fiber alignment

A uniform threshold filter was applied to representative SEM images to eliminate contrast and brightness bias among images. Using ImageJ software (NIH, Bethesda, Maryland, USA), SEM images (in triplicate) were transformed into power spectra using Fast Fourier Transform (FFT) analysis. A 90° shift was performed on all power spectra to correct for the transformation that is mathematically inherent to FFT. The angle at which the peak appears directly correlates to the principal axis of fiber orientation. Based on the power spectra, a radial summation of pixel intensity from 0–360° in 1° increments was conducted using the Oval Profile plugin (O'Connell, 2002). Given the horizontally symmetric nature of FFTs, only the data from 0–180° was plotted. The pixel intensity values were normalized and plotted against the angle of acquisition. The angle of fiber orientation was determined from the location of the peaks on the intensity plots. The alignment of the sample was determined from the peak characteristics, where the greatest intensity increase over the smallest degree range signified the highest degree of fiber alignment.

### 2.7. Determination of fiber diameter

The diameters of 25 nanofibers were measured from representative 512 × 512 pixel SEM images at 8000× magnification using ImageJ. This procedure was repeated for 6 different images per condition to ensure statistical significance. One-way analysis of variance (ANOVA) was performed and a two-tailed $t$-test used to determine statistical significance between samples. The significance was determined at $p < 0.05$.

### 2.8. Quantification of nanofiber diameter distribution for HTP-CES versus ES

The diameters of 50 nanofibers were measured from representative 512 × 512 pixel SEM images of fibers spun using the HTP-CES system and the ES system at 8000× magnification using ImageJ. The nanofiber diameters were plotted against the number of nanofibers in the given diameter range to yield histograms showing the diameter distributions.

## 3. Results

### 3.1. Effect of polymer concentration on morphology of nanofibers

Scanning electron micrographs of aligned C-PCL nanofibers fabricated by the HTP-CES from four polymer solutions of different ratios of chitosan to PCL are shown in Fig. 2a. Nanofibers fabricated from all four polymer solutions exhibited bead-free morphologies. C-PCL nanofibers composed of 10 wt% chitosan and 90 wt% PCL (10/90C-PCL) showed the most uniform fibrous structure with no visible branching. Increasing the chitosan concentration (25/75C-PCL) resulted in less uniform nanofiber morphologies with slight diameter variations. Further increases in chitosan concentration (75/25C-PCL and 90/10C-PCL) resulted in the formation of a significant, branched sub-structures, and thus less uniform nanofibers in terms of morphology. Thus, the 25/75C-PCL solution was chosen as the optimal concentration for all subsequent experiments because the resultant nanofibers exhibited the most uniform structure at the highest chitosan concentration, which is important for biological applications.

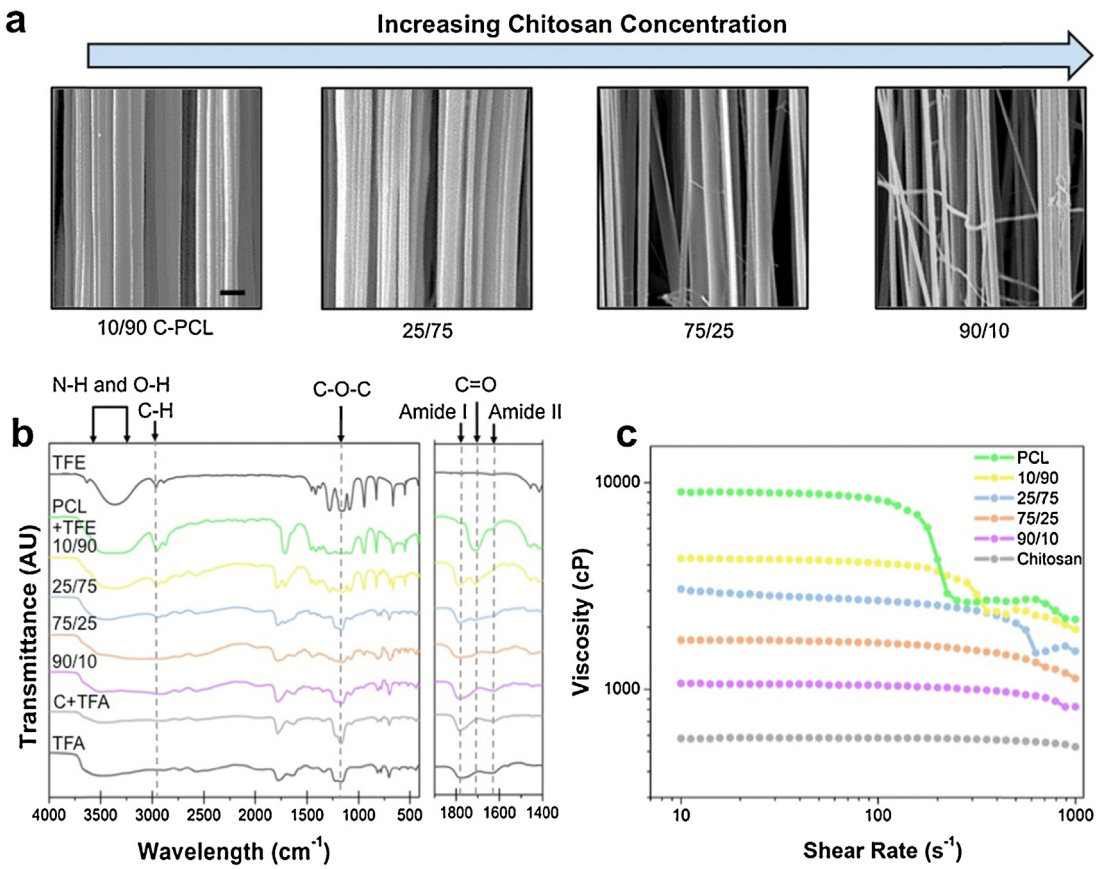


**Fig. 2.** Nanofiber morphology and physicochemical properties of C-PCL polymer blend solutions. (a) Fiber morphology characterized by SEM. From left to right, the chitosan concentration in the blended copolymer nanofibers was increased. An increase in a branched sub-structure corresponding with less uniform nanofiber morphology was observed with an increase in chitosan concentration. The scale bar represents 750 nm. (b) FTIR analysis of solvents, pure polymer stock solutions, and polymer blends. (c) Rheological properties of pure polymer stock and polymer blend solutions.

The FTIR spectra for stock chitosan (C + TFA) and PCL (PCL + TFE) solutions as well as blends of the two solutions are shown in Fig. 2b. In the spectrum of C + TFA, the presence of chitosan is confirmed by characteristic peaks of chitosan at 1790 $cm^{-1}$ (C=O, amide I), 1635 $cm^{-1}$ (—CONH, amide II), and at 1080 $cm^{-1}$ (—C—O—C). The presence of TFA is confirmed by three bands due to C—F stretching vibrations (815–705 $cm^{-1}$) (Hasegawa, Isogai, Onabe, & Usuda, 1992). The broad peaks of C + TFA at 3450 $cm^{-1}$ is from the overlapping N—H and O—H stretching vibrations (Shalumon et al., 2010). In the spectra of PCL + TFE, the presence of PCL is confirmed by the peaks at 2960 and 1710 $cm^{-1}$ corresponding to C—H and C=O stretching vibrations, respectively. The broad band around 1200 $cm^{-1}$ is attributed to the overlapping of C—O—C stretching of PCL with C—O stretching of TFE.

As the concentration of chitosan decreases for the blend polymer solutions, the chitosan characteristic peaks at 1790 $cm^{-1}$ (amide I) and 1635 $cm^{-1}$ (amide II) decrease and eventually disappear when there is no chitosan, whereas the peak at 1710 $cm^{-1}$ attributed to PCL increases and becomes dominant. In addition, the chitosan C—O—C peak at 1080 $cm^{-1}$ broadens slightly towards 1200 $cm^{-1}$ where the C—O—C stretching vibration peaks of PCL and C—O stretching peak of TFE are observed on the PCL + TFE spectrum. When chitosan concentration increases, the peak at 2960 $cm^{-1}$ assigned to C—H stretching in PCL diminishes (Sahoo, Sasmal, Nanda, Phani, & Nayak, 2010). The characteristic peaks of the pure stock solutions are identifiable and no additional peaks are present, indicating the chemical structure of chitosan and PCL remain unchanged with no additional compounds formed when blended to yield the electrospinning solutions.

The viscosity of the polymer solutions plays a significant role in solution spinnability and the resultant nanofiber morphology. Fig. 2c shows the viscosity versus shear rate for the pure polymer stock and blend solutions. The chitosan-TFA stock solution has the lowest viscosity and experiences very little shear thinning as the shear rate is increased. When the chitosan-TFA is blended with 10% PCL-TFE solution, the viscosity increases and shear thinning occurs as the shear rate increases to 1000 $s^{-1}$. Further increases in PCL-TFE concentration in the blend increases the viscosity, but induces shear thinning at lower shear rates. The stock PCL-TFE solution shows the most drastic shear thinning beginning at 150 $s^{-1}$ and leveling out until further thinning effects are seen at 700 $s^{-1}$. The viscosities for all C-PCL blend curves fall between the viscosities of the pure polymer stock solutions, indicating the two solutions are miscible and form a single phase upon mixing.

### 3.2. *Effect of centrifugal force on nanofiber alignment (HTP-CES versus ES)*

The HTP-CES system highlighted in Fig. 1 was utilized as both a centrifugal-electrospinning (HTP-CES) system and a conventional electrospinning (ES) system where centrifugal forces were not applied. SEM micrographs in Fig. 3a depict the morphological differences between nanofibers spun with and without the influence of centrifugal force. Nanofibers produced by HTP-CES are homogeneous in diameter and aligned vertically, whereas substantial branching and fiber diameter non-uniformity is observed in nanofibers produced by ES. Fast Fourier Transform (FFT) analysis was used to quantify differences in nanofiber alignment, and the resultant FFT power spectra are shown in Fig. 3b. A distinct pixel

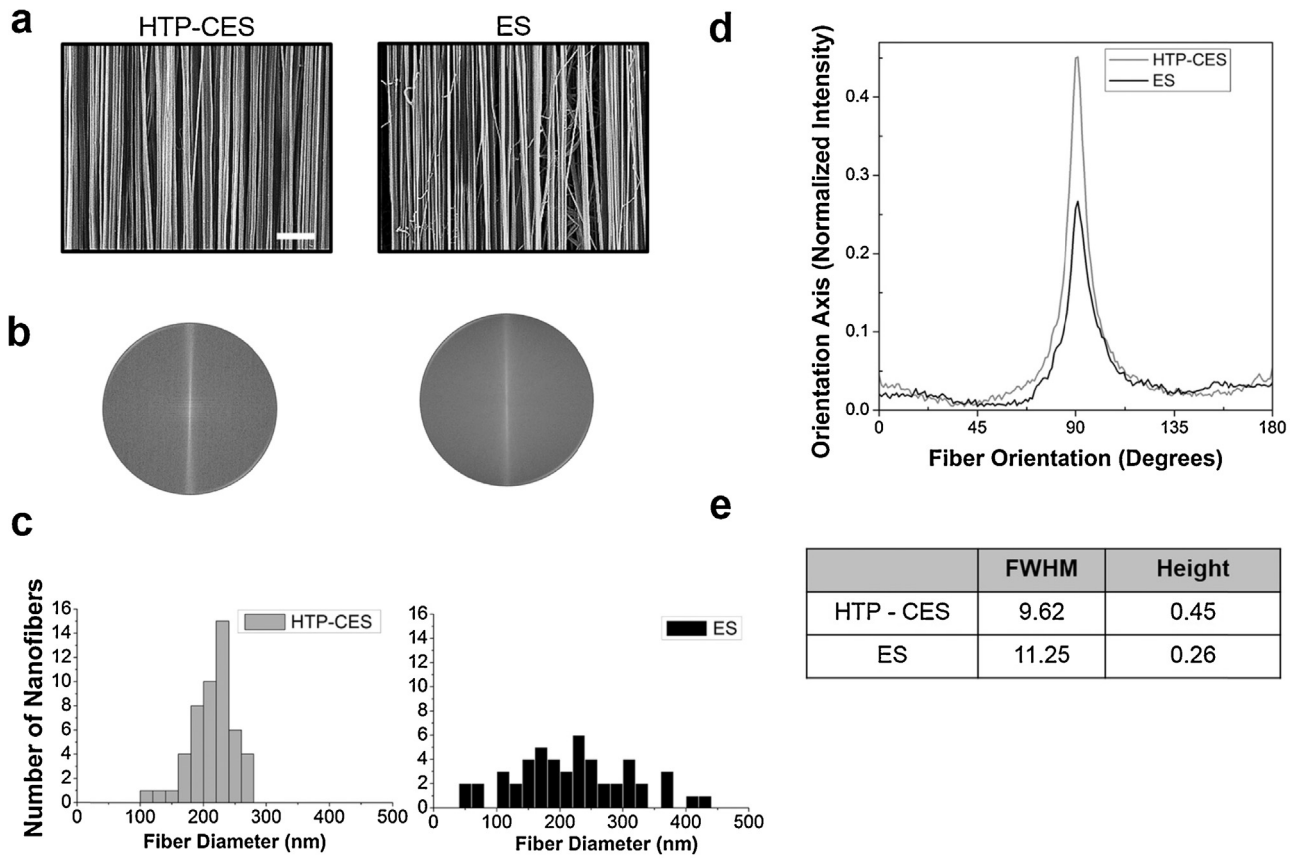


| | FWHM | Height |
|---|---|---|
| HTP - CES | 9.62 | 0.45 |
| ES | 11.25 | 0.26 |

**Fig. 3.** The effect of centrifugal force on fiber morphology and alignment. (a) SEM images of centrifugally electrospun (HTP-CES) versus electrospun (ES) nanofibers showing morphological differences. The scale bar represents 5 μm. (b) FFT power spectra based on SEM images of HTP-CES versus ES nanofibers. (c) Histograms of nanofiber diameter distributions for HTP-CES versus ES nanofibers. (d) The normalized radial summation of pixel intensity versus degree of acquisition of FFT power spectra. (e) Quantitative FFT results for HTP-CES versus ES nanofibers including values for the Full Width Half Maximum (FWHM) and peak height corresponding to normalized intensity.

intensity increase along the axis of fiber orientation at 90° confirms nanofiber alignment for both samples. The diameter distributions of nanofibers produced using the two systems were compared by histograms (Fig. 3c). Nanofibers spun using conventional electrospinning (ES) ranged in diameter from approximately 25–450 nm whereas the nanofiber diameter distribution for samples spun in the presence of centrifugal forces (HTP-CES) was narrower and more uniform ranging from approximately 100 nm to 275 nm. This indicates that the HTP-CES system produces nanofibers with superior uniformity.

The Oval Profile plugin (O'Connell, 2002) was used to generate a normalized plot from 0–180° (Fig. 3d). Sample alignment was quantified using the peak characteristics, where the greatest increase in normalized intensity over the smallest degree range signifies the highest degree of fiber alignment. The peaks associated with HTP-CES and ES conditions show a similar width, yet the peak height in normalized intensity for the HTP-CES samples (0.45) was greater than that of the ES samples (0.26) (Fig. 3e). The Full Width Half Maximum (FWHM) or peak width at half the maximum height was used as a quantitative measure of alignment where a smaller value signifies a narrower peak and thus better alignment. The FWHM is smaller for HTP-CES (9.62) than for ES (11.25) indicating that the HTP-CES system results in better alignment than conventional ES (Fig. 3e).

### 3.3. Effect of needle gauge on nanofiber diameter

SEM images were used to measure and evaluate the diameters of nanofibers produced using five different needle gauges (18, 21, 24, 27, 30-gauge) with the HTP-CES system. All operating parameters were held constant while the needle guage was varied to determine a correlation between needle diameter and nanofiber diameter. A concave relationship between nanofiber diameter and needle diameter was identified (Fig. 4a and b). The smallest average fiber diameter and the narrowest fiber diameter distribution was achieved using a 24-gauge needle. As the needle gauge was either increased or decreased, a larger fiber diameter and a wider diameter distribution was observed in conjunction with a larger standard deviation.

### 3.4. Effect of needle gauge on nanofiber alignment

The relationship between needle gauge and nanofiber alignment was investigated using the three smallest needle gauge conditions (24-, 27- and 30-gauge) due to superior overall morphology and diameter uniformity of nanofibers produced using these needle gauges. Samples associated with all three needle gauges exhibited high degrees of alignment (Fig. 5a). Using the Oval Profile plugin (O'Connell, 2002), the power spectra (Fig. 5b) was plotted from 0–180° and normalized (Fig. 5c). The FFT power spectra associated with all conditions show a distinct pixel intensity increase in the vertical direction indicating fiber alignment. Further, the normalized intensity versus fiber orientation plot shows three distinct and narrow peaks centered around 90°. To quantify and compare the fiber alignment among samples, the peak heights and the Full Width Half Maximum (FWHM) values were calculated (Fig. 5d). As previously mentioned, the best alignment was determined from the peak characteristics, where the greatest increase in normalized

a

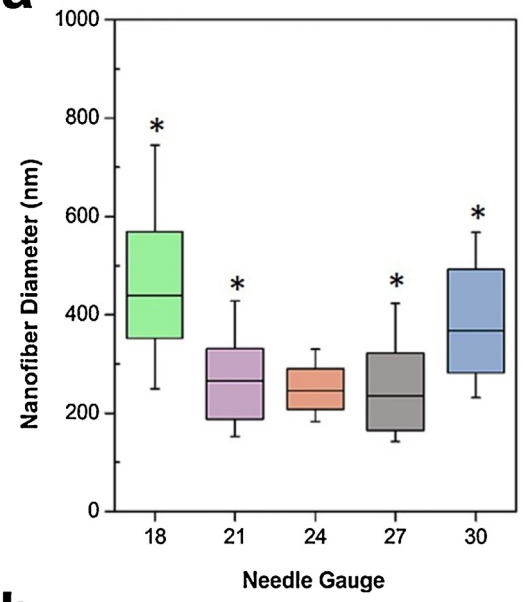


b

| Needle Gauge | Needle ID (mm) | Mean Diameter ± Deviation (nm) | | |
|---|---|---|---|---|
| 18 | 0.84 | 477 | ± | 201 |
| 21 | 0.51 | 275 | ± | 102 |
| 24 | 0.31 | 253 | ± | 61 |
| 27 | 0.21 | 261 | ± | 119 |
| 30 | 0.16 | 389 | ± | 138 |

**Fig. 4.** C-PCL nanofibers produced using various needle gauges. (a) Box plot of nanofiber diameter distribution for five needle gauges showing concave relationship between needle gauge and nanofiber diameter. (*$p < 0.05$ as compared with the 24-gauge condition). (b) Summary of needle gauge/needle inner diameter versus average nanofiber diameter.

intensity over the smallest degree range, as represented by FWHM, signifies the highest degree of fiber alignment. The nanofibers produced using the 24-gauge needle exhibited the highest peak followed by the 30-gauge and 27-gauge fibers. The FWHM value was smallest for the 24-gauge sample (8.60), followed by the 30-gauge sample (12.63), and the 27-gauge sample (13.37). Using these quantitative measures, the 24-gauge needle exhibited the highest degree of alignment and the 27-gauge needle exhibited the lowest.

## 4. Discussion

Synthetic and natural polymer blend nanofibers are playing an increasingly important role in many engineering applications, but are challenging to fabricate due to poor miscibility between component polymers (Bhattarai et al., 2009). Centrifugal spinning has been primarily used to fabricate micron-scale C-PCL fibers (Cardoso, Machado-Silva, Sabino, Santos, & Zavaglia, 2014), yet traditional electrospinning remains the dominant technique for fabrication of C-PCL nanofibers. Here we present a technology, the HTP-CES system, which allows for production of homogenous, highly-aligned chitosan-polycaprolactone (C-PCL) nanofibers.

Initially, various C-PCL blends were evaluated to determine optimal polymer blend compositions in terms of nanofiber morphology and uniformity, where a higher chitosan concentration yields a more relevant material for biological applications. The effect of natural versus synthetic polymer properties on resultant fibers is evident in Fig. 2a where nanofibers containing a large proportion of PCL (10/90C-PCL) exhibit the most uniform fibrous structures with no visible branching. This might be due to synthetic polymers generally containing fewer entanglements than natural polymers, such as chitosan so that they are more uniform and easily electrospun. Additionally, PCL dissolved in TFE is highly viscous and exhibits strong non-Newtonian shear thinning properties. The shear thinning of the PCL solution allows the polymer chains to interact and align under the centrifugal force so that less branched and more uniform nanofibers are produced. After visual evaluation of the morphology of resultant C-PCL blend nanofibers, 25/75C-PCL was chosen as the optimal composition due to the overall nanofiber uniformity and the need to maximize chitosan content and thus was used for all subsequent experiments.

The advantage of centrifugal force application on nanofiber alignment was demonstrated by electrospinning C-PCL solution with (1) a stationary spinneret (ES) and (2) a spinneret rotated at 108 rpm (CES). All other operating parameters were held constant; however, the polymer solution flow rate was different due to the difference in centrifugal versus gravity feed. Using FFT for quantification of fiber alignment, and SEM imaging for visualization of fiber morphology, it is clear that the addition of centrifugal force increases nanofiber alignment (Fig. 3a). The high degree of fiber alignment achieved using the HTP-CES occurs via the exploitation of two mechanisms. First, the collector functions as an array of parallel electrodes, where nanofibers selectively align across the insulating gap between two neighboring electrodes (Fig. 1a and b). Second, the centrifugal feed disperses the fibers perpendicular to each wire. Additionally, the centrifugal force imparted by the HTP-CES system on the polymer jet results in additional cohesive forces within the jet that prevent splaying and allows for an increased stretching and elongation region. This leads to a more uniform nanofiber diameter distribution (Fig. 3c).

In addition to alignment, strict control over nanofiber diameter is highly desirable. The complex interplay among process parameters, fluid dynamics, electrodynamics, and solution rheology associated with electrospinning often means that it is difficult to correlate the effects of specific operating parameters with nanofiber properties. Studies have demonstrated a variety of relationships between the needle diameter and resultant nanofiber diameter, including direct (Heikkila & Harlin, 2008; Ko, Bhullar, Mohtaram, Willerth, & Jun, 2014; Zhao, Wu, Wang, & Huang, 2004), inverse (Cui, Li, Zhou, & Weng, 2007), concave (Wang, Zhang, Huang, Yan, & Su, 2006), and convex (Macossay, Marruffo, Rincon, Eubanks, & Kuang, 2007) correlations. These studies indicate that extracting the relationship between needle diameter and nanofiber diameter is difficult especially because many polymeric electrospinning solutions are non-Newtonian fluids (Kim, Kim, Kang, Marquez, & Joo, 2006; Theron, Zussman, & Yarin, 2004; Zhou, Green, & Joo, 2006). Because the HTP-CES system has an added centrifugal feed component that enhances nanofiber uniformity and alignment, it is possible to spin bead-free fibers over a wider range of needle gauges than is generally possible in a conventional electrospinning system. Here, a concave correlation between needle gauge and fiber diameter is identified for our system (Fig, 4a and b) where other critical parameters such as operating voltage, solution concentration, and spinneret rotational speed are all held constant.

The concave correlation between needle diameter and resultant fiber diameter indicates that two different instability regimes within the polymer jet are present. In the first regime, where the polymer solution is centrifugally electrospun through a decreasing

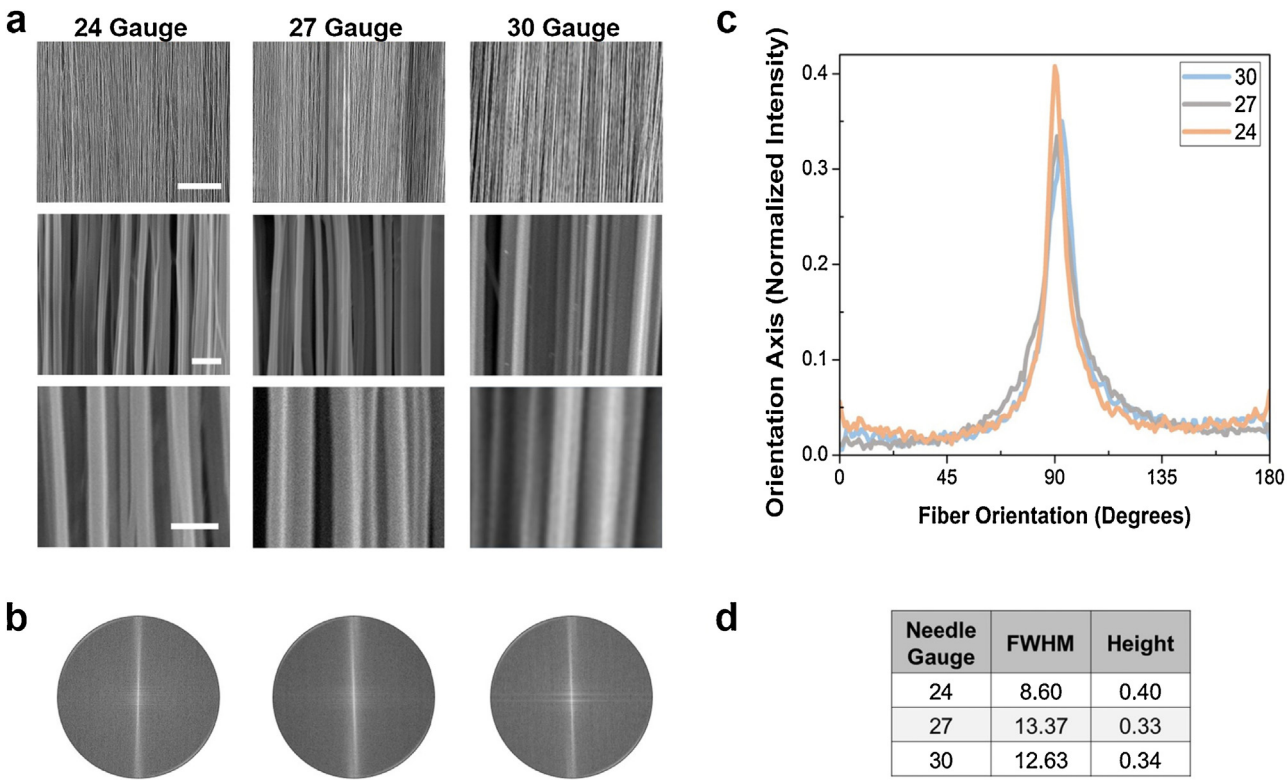


| Needle Gauge | FWHM | Height |
|---|---|---|
| 24 | 8.60 | 0.40 |
| 27 | 13.37 | 0.33 |
| 30 | 12.63 | 0.34 |

**Fig. 5.** Effect of needle gauge on nanofiber alignment. (a) SEM images of nanofibers electrospun using 24, 27, and 30-gauge needles. In the top row of images, the scale bar represents 50 μm. Scale bars for the middle and bottom rows represent 1 μm and 500 nm, respectively. (b) The power spectra representing each needle gauge as obtained using FFT (indicates which spectrum is for which needle size from left to right). (c) The normalized radial summation of pixel intensity versus degree of acquisition for each FFT for alignment comparisons. (d) Full width half maximum (FWHM), and peak height quantification.

needle diameter (18, 21, and 24-gauge), the 25/75C-PCL solution experiences shear thinning in response to the increased shear force. This aligns the polymer chains, thereby decreases solution viscosity. In this regime, the fiber diameter decreases as the needle diameter decreases due to the alignment and conformity of the polymer chains.

In the second regime, where the centrifugal force becomes more prominent and the needle diameter is further decreased (24, 27, and 30-gauge), the shear thinning behavior of polymer solutions and electrostatic forces are no longer great enough to promote formation of a stable Taylor cone. Upon decreasing the needle diameter, the orifice size becomes too restricted to continuously produce fibers and the increase in the shear force begins to deform the polymer. Here, the viscoelastic properties of the polymer solution result in swelling of the jet upon exiting the restriction. This has also been observed in other studies where polymer solutions are exposed to high shear stresses (Hao et al., 2014; Zhang et al., 2006). The polymer solution jet has a decreased flow rate and a thicker jet is formed resulting in thicker fibers.

Whereas, the 24-gauge samples were optimal, samples produced using all needle gauges were composed of fibers on the order of hundreds of nanometers with standard deviations of approximately 200 nm or less, demonstrating the versatility of the HTP-CES. Using the HTP-CES, it is possible to obtain nanofibers in a defined diameter range by simply changing the needle gauge on the spinneret and leaving all other operating parameters constant.

Nanofibers produced using the three smallest needle gauges (24, 27, and 30-gauge) showed the lowest degree of branching as observed via SEM and were analyzed to characterize the effect of needle gauge on alignment. The greatest degree of alignment occurred in samples produced using the 24-gauge needle (8.60), followed by the 30-gauge (12.63) and finally, the 27-gauge samples (13.37) (Fig. 5c and d). Coupling the diameter and alignment analyses, we conclude that the 24-gauge needle provides the narrowest nanofiber diameter distribution with the best alignment, thereby making it the optimal condition for spinning of 25/75C-PCL using the HTP-CES.

## 5. Conclusion

A nanofiber yield near 75% renders the HTP-CES system convenient for generation and collection of a sizeable number of samples concurrently. Our approach proved to be superior to conventional electrospinning in terms of nanofiber morphology, uniformity, and alignment. The superior morphology of C-PCL nanofibers can be attributed to the addition of the centrifugal force imparted on the polymer solution by the HTP-CES. The unique centrifugal force induces shear thining solution behavior while imparting tangential and axial stretching forces onto the nanofibers, minimizing the "whipping region" and depositing highly uniform fibers under conditions not attainable by conventional electrospinning. The optimal centrifugal-electrospinning condition for producing uniform, highly-aligned 25/75C-PCL nanofibers was found to be a 24-gauge needle with 5 kV operation voltage rotating at 108 rpm. All nanofiber samples analyzed exhibited a narrow diameter distribution with standard deviations of 200 nm or less and distinct FFT alignment peaks centered around 90°. The fabrication of aligned nanofibers with specified diameters as demonstrated here is critical in the biomedical and piezoelectric device industries, where uniformity and high degrees of alignment are required.

## Acknowledgements

This work is supported in part by NIH grant NIH/NCI R01CA172455 and Kyocera Professor Endowment to M.Z. A.E.E. acknowledges support from the National Science Foundation Grad-

uate Research Fellowship Program. S.L.L. acknowledges support from the Ruth L. Kirschstein NIH Training grant T32CA138312. We acknowledge the use of resources at the Center for Nanotechnology at the University of Washington.

## References


Baji, A., Mai, Y. W., Wong, S. C., Abtahi, M., & Chen, P. (2010). Electrospinning of polymer nanofibers: effects on oriented morphology, structures and tensile properties. *Composites Science and Technology*, *70*(5), 703–718. http://dx.doi.org/10.1016/j.compscitech.2010.01.010

Bhattarai, N., Li, Z. S., Gunn, J., Leung, M., Cooper, A., Edmondson, D., & Zhang, M. Q. (2009). Natural-synthetic polyblend nanofibers for biomedical applications. *Advanced Materials*, *21*(27), 2792–2797. http://dx.doi.org/10.1002/adma.200802513

Balamurugan, R., Sundarrajan, S., & Ramakrishna, S. (2011). Recent trends in nanofibrous membranes and their suitability for air and water filtrations. *Membranes*, *1*, 232–248. http://dx.doi.org/10.3390/membranes1030232

Cooper, A., Bhattarai, N., & Zhang, M. Q. (2011). Fabrication and cellular compatibility of aligned chitosan-PCL fibers for nerve tissue regeneration. *Carbohydrate Polymers*, *85*(1), 149–156. http://dx.doi.org/10.1016/j.carbpol.2011.02.008

Cooper, A., Jana, S., Bhattarai, N., & Zhang, M. Q. (2010). Aligned chitosan-based nanofibers for enhanced myogenesis. *Journal of materials chemistry*, *20*(40), 8904–8911. http://dx.doi.org/10.1039/c0jm01841d

Cardoso, G. B. C., Machado-Silva, A. B., Sabino, M., Santos, A. R., Jr., & Zavaglia, C. A. C. (2014). Novel hybrid membrane of chitosan/poly(-caprolactone) for tissue engineering. *Biomatter*, *4*(1), e29508. http://dx.doi.org/10.4161/biom.29508

Chang, J., Dommer, M., Chang, C., & Lin, L. (2012). Piezoelectric nanofibers for energy scavenging applications. *Nano Energy*, *1*, 356–371.

Cui, W., Zhou, Y., & Chang, J. (2010). Electrospun nanofibrous materials for tissue engineering and drug delivery. *Science and Technology of Advance Materials*, *11*, 14108. http://dx.doi.org/10.1088/1468-6996/11/1/014108

Cui, W. G., Li, X. H., Zhou, S. B., & Weng, J. (2007). Investigation on process parameters of electrospinning system through orthogonal experimental design. *Journal of Applied Polymer Science*, *103*(5), 3105–3112. http://dx.doi.org/10.1002/App.25464

D'Arcy, J. M., El-Kady, M. F., Khine, P. P., Zhang, L. H., Lee, S. H., Davis, N. R., & Kaner, R. B. (2014). Vapor-phase polymerization of nanofibrillar poly(3,4-ethylenedioxythiophene) for supercapacitors. *ACS Nano*, *8*(2), 1500–1510. http://dx.doi.org/10.1021/Nn405595r

Edmondson, D., Cooper, A., Jana, S., Wood, D., & Zhang, M. (2012). Centrifugal electrospinning of highly aligned polymer nanofibers over a large area. *Journal of Materials Chemistry*, *22*, 18646–18652.

Ghasemi-Mobarakeh, L., Prabhakaran, M. P., Morshed, M., Nasr-Esfahani, M.-H., & Ramakrishna, S. (2008). Electrospun poly(3-caprolactone)/gelatin nanofibrous scaffolds for nerve tissue engineering. *Biomaterials*, *29*, 4532–4639.

Guo, Q., Zhou, X., Li, X., Chen, S., Seema, A., Greiner, A., & Hou, H. (2009). Supercapacitors based on hybrid carbon nanofibers containing multiwalled carbon nanotubes. *Journal of Materials Chemistry*, *19*(18), 2810–2816.

Hasegawa, M., Isogai, A., Onabe, F., & Usuda, M. (1992). Dissolving states of cellulose and chitosan in trifluoroacetic-acid. *Journal of Applied Polymer Science*, *45*(10), 1857–1863. http://dx.doi.org/10.1002/app.1992.070451020

Heikkila, P., & Harlin, A. (2008). Parameter study of electrospinning of polyamide-6. *European Polymer Journal*, *44*(10), 3067–3079. http://dx.doi.org/10.1016/j.eurpolymj.2008.06.032

Hiralal, P., Imaizumi, S., Unalan, H. E., Matsumoto, H., Minagawa, M., Rouvala, M., & Amaratunga, G. A. J. (2010). Nanomaterial-enhanced all-solid flexible zinc-carbon batteries. *ACS Nano*, *4*(5), 2730–2734. http://dx.doi.org/10.1021/nn901391q

Hao, W. T., Fang, C. P., Yu, J. X., Zhang, L., Xue, T., & Yang, W. (2014). Polyurethane electrospun mats strengthened and toughened by physically blended polyhedral oligomeric silsesquioxane. *Journal of Applied Polymer Science*, *131*(20), 40902. http://dx.doi.org/10.1002/A40902

Ignatious, F., Sun, L., Lee, C.-P., & Baldoni, J. (2010). Electrospun nanofibers in oral drug delivery. *Pharmaceutical Research*, *27*(4), 576–588. http://dx.doi.org/10.1007/s11095-010-0061-6

Jirsak, O., Sysel, P., Sanetrnik, F., Hruza, J., & Chaloupek, J. (2010). Polyamic acid nanofibers produced by needleless electrospinning. *Journal of Nanomaterials*, *2010*, 842831. http://dx.doi.org/10.1155/2010/842831

Kumar, A., Wei, M., Barry, C., Chen, J., & Mead, J. (2010). Controlling fiber repulsion in multijet electrospinning for higher throughput. *Macromolecular Materials and Engineering*, *295*, 701–708.

Kim, C. W., Kim, D. S., Kang, S. Y., Marquez, M., & Joo, Y. L. (2006). Structural studies of electrospun cellulose nanofibers. *Polymer*, *47*(14), 5097–5107. http://dx.doi.org/10.1016/j.polymer.2006.05.033

Ko, J., Bhullar, S. K., Mohtaram, N. K., Willerth, S. M., & Jun, M. B. G. (2014). Using mathematical modeling to control topographical properties of poly (epsilon-caprolactone) melt electrospun scaffolds. *Journal of Micromechanics and Microengineering*, *24*(6) http://dx.doi.org/10.1088/0960-1317/24/6/065009

Lukas, D., Sarkar, A., & Pokorny, P. (2008). Self-organization of jets in electrospinning from free liquid surface: a generalized approach. *Journal of Applied Physics*, *103*, 84309.

Li, D., Wang, Y. L., & Xia, Y. N. (2004). Electrospinning nanofibers as uniaxially aligned arrays and layer-by-layer stacked films. *Advanced Materials*, *16*(4), 361–366. http://dx.doi.org/10.1002/adma.200306226

Macossay, J., Marruffo, A., Rincon, R., Eubanks, T., & Kuang, A. (2007). Effect of needle diameter on nanofiber diameter and thermal properties of electrospun poly(methyl methacrylate). *Polymers for Advanced Technologies*, *18*(3), 180–183. http://dx.doi.org/10.1002/Pat.844

Matthews, J. A., Wnek, G. E., Simpson, D. G., & Bowlin, G. L. (2002). Electrospinning of collagen nanofibers. *Biomacromolecules*, *3*(2), 232–238. http://dx.doi.org/10.1021/Bm015533u

O'Connell, B., 2002. Oval Profile Plot. In: ImageJ. Bethesda, MD : U.S. National Institutes of Health. <http://rsbweb.nih.gov/ij/plugins/ovalprofile.html>

Patel, S., Kurpinski, K., Quigley, R., Gao, H., Hsiao, B. S., Poo, M.-M., & Li, S. (2007). Bioactive nanofibers: synergistic effects of nanotopography and chemical signaling on cell guidance. *Nano letters*, *7*(7), 2122–2128.

Ramakrishna, S., Fujihara, K., Teo, W.-E., Yong, T., Ma, Z., & Ramaseshan, R. (2006). Electrospun nanofibers: solving global issues. *Materials Today*, *9*(3), 40–50.

Sionkowska, A. (2011). Current research on the blends of natural and synthetic polymers as new biomaterials: review. *Progress in Polymer Science*, *36*(9), 1254–1276. http://dx.doi.org/10.1016/j.progpolymsci.2011.05.003

Suzuki, A., Hosoi, K., & Miyagi, K. (2015). Broad poly(ethylene terephthalate) nanofiber sheet prepared by $CO_2$ laser supersonic continuous multi-drawing. *Polymer*, *60*, 252–259. http://dx.doi.org/10.1016/j.polymer.2014.11.064

Shalumon, K. T., Anulekha, K. H., Girish, C. M., Prasanth, R., Nair, S. V., & Jayakumar, R. (2010). Single step electrospinning of chitosan/poly(caprolactone) nanofibers using formic acid/acetone solvent mixture. *Carbohydrate Polymers*, *80*(2), 413–419. http://dx.doi.org/10.1016/j.carbpol.2009.11.039

Sahoo, S., Sasmal, A., Nanda, R., Phani, A. R., & Nayak, P. L. (2010). Synthesis of chitosan–polycaprolactone blend for control delivery of ofloxacin drug. *Carbohydrate Polymers*, *79*(1), 106–113. http://dx.doi.org/10.1016/j.carbpol.2009.07.042

Theron, A., Zussman, E., & Yarin, A. L. (2001). Electrostatic field-assisted alignment of electrospun nanofibres. *Nanotechnology*, *12*(3), 384–390.

Thoppey, N. M., Bochinski, J. R., Clarke, L. I., & Gorga, R. E. (2011). Edge electrospinning for high throughput production of quality nanofibers. *Nanotechnology*, *22*(34) http://dx.doi.org/10.1088/0957-4484/22/34/345301

Theron, S. A., Zussman, E., & Yarin, A. L. (2004). Experimental investigation of the governing parameters in the electrospinning of polymer solutions. *Polymer*, *45*(6), 2017–2030.

Varesano, A., Rombaldoni, F., Mazzuchetti, G., Tonina, C., & Comottob, R. (2010). Multi-jet nozzle electrospinning on textile substrates: observations on process and nanofibremat deposition. *Polymer International*, *59*, 1606–1615.

Varabhas, J. S., Chase, G. G., & Reneker, D. H. (2008). Electrospun nanofibers from a porous hollow tube. *Polymer*, *49*(19), 4226–4229. http://dx.doi.org/10.1016/j.polymer.2008.07.043

Wang, C., Zhang, W., Huang, Z. H., Yan, E. Y., & Su, Y. H. (2006). Effect of concentration, voltage, take-over distance and diameter of pinhead on precursory poly(phenylene vinylene) electrospinning. *Pigment & Resin Technology*, *35*(5), 278–283. http://dx.doi.org/10.1108/03699420610692887

Wan, Y. Z., Hu, D., Xiong, G. Y., Li, D. Y., Guo, R. S., & Luo, H. L. (2015). Directional fluid induced self-assembly of oriented bacterial cellulose nanofibers for potential biomimetic tissue engineering scaffolds. *Materials Chemistry and Physics*, *149*, 7–11. http://dx.doi.org/10.1016/j.matchemphys.2014.10.037

Wan, Y. Z., Yang, Z. W., Xiong, G. Y., Raman, S. R., & Luo, H. L. (2015). Bacterial cellulose-templated synthesis of free-standing silica nanotubes with a three-dimensional network structure. *RSC Advances*, *5*(60), 48875–48880. http://dx.doi.org/10.1039/C5ra08658b

Yin, Z., Chen, X., Chen, J. L., Shen, W. L., Nguyen, T. M. H., Gao, L., & Ouyang, H. W. (2010). The regulation of tendon stem cell differentiation by the alignment of nanofibers. *Biomaterials*, *31*(8), 2163–2175. http://dx.doi.org/10.1016/j.biomaterials.2009.11.083

Zhang, H., Liu, X., Yang, M., & Zhu, L. (2015). Silk fibroin/sodium alginate composite nano-fibrous scaffold prepared through thermally induced phase-separation (TIPS) method for biomedical applications. *Materials Science and Engineering C*, *55*, 8–13.

Zhou, H. J., Green, T. B., & Joo, Y. L. (2006). The thermal effects on electrospinning of polylactic acid melts. *Polymer*, *47*(21), 7497–7505. http://dx.doi.org/10.1016/j.polymer.2006.08.042

Zahedia, P., Rezaeiana, I., Ranaei-Siadatb, S.-O., Jafaria, S.-H., & Supapholc, P. (2012). A review on wound dressings with an emphasis on electrospun nanofibrous polymeric bandages. *Polymer of Advance Technology*, *21*, 77–95. http://dx.doi.org/10.1002/pat.1625

Zhao, S. L., Wu, X. H., Wang, L. G., & Huang, Y. (2004). Electrospinning of ethyl-cyanoethyl cellulose/tetrahydrofuran solutions. *Journal of Applied Polymer Science*, *91*(1), 242–246. http://dx.doi.org/10.1002/App.13196

Zhang, Y. Z., Wang, X., Feng, Y., Li, J., Lim, C. T., & Ramakrishna, S. (2006). Coaxial electrospinning of (fluorescein isothiocyanate-conjugated bovine serum albumin)-encapsulated poly(epsilon-caprolactone) nanofibers for sustained release. *Biomacromolecules*, *7*(4), 1049–1057. http://dx.doi.org/10.1021/Bm050743i